Optical Materials 126 (2022) 112203

Contents lists available at ScienceDirect

Optical Materials

journal homepage: www.elsevier.com/locate/optmat

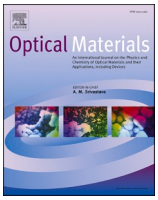

Femtosecond-laser processing incubation in Diamond-like carbon

Lucas K. Nolasco [a,c], Flávio P. Almeida [a], Gustavo F.B. Almeida [a,b], Juliana M.P. Almeida [c,d], Valmor R. Mastelaro [a], Kelly T. Paula [a], Cleber R. Mendonça [a,*]

[a] São Carlos Institute of Physics, University of São Paulo, 13560-970, São Carlos, SP, Brazil
[b] Institute of Physics, Federal University of Uberlândia, PO Box 593, 38400-902, Uberlândia, MG, Brazil
[c] Department of Materials Engineering, São Carlos School of Engineering, University of São Paulo, 13563-120, São Carlos, SP, Brazil
[d] Physics Department - CCET Federal University of São Carlos, CEP 13565-905, São Carlos, SP, Brazil

ARTICLE INFO

Keywords:
Diamond-like carbon
Micromachining
Incubation
Femtosecond laser

ABSTRACT

Diamond-like carbon (DLC) has been commercialized as an advanced material for combining diamond and graphite properties with other material systems, with ease of processing and reduced costs. DLC has been broadly studied as an interesting material for applications ranging from biology to optics, passing through mechanics and electronics. Hence, for given applications, complex patterning of DLC is required, which can be accomplished by conventional lithographic approaches, as well as laser structuring. In this way, this paper focuses on studying the incubation process, the dependence of the threshold fluence with the number of irradiated pulses, on the fs-laser microstructuring of DLC films. We determined a single pulse fluence of (1.0 ± 0.1) J/cm^2, a value that decreases to a plateau of (0.13 ± 0.04) J/cm^2 for a large number of pulses. The slow evolution of the fluence threshold with the number of pulses indicates a low incubation parameter, such that a large number of pulses is required to damage the material. By modeling the single-pulse damage threshold fluence considering multiphoton and avalanche ionization, we were able to estimate a two-photon absorption cross-section for DLC of $(1.5 \pm 0.5) \times 10^{-60}$ m^{4}s^{1}photon^{-1}, which is consistent with the one known for diamond. Finally, Raman spectroscopy of the fs-laser processing DLC sample indicates a decrease of the sp^3 fraction and a more ordered phase.

1. Introduction

Diamond-like carbon (DLC) is a metastable form of amorphous carbon containing a significant fraction of sp^3 bonds [1], some terminated by hydrogen (amorphous hydrogenated carbon, a-C:H), that has attracted scientific interest in recent years due to its unique properties, referring to the combination of typical properties of diamond and graphite [2]. The nature of the DLC depends very much on the deposition process, the geometric organization, and the predominant type of hybridization of carbon atoms. By controlling the processing parameters, DLC offers advantages over diamond films, such as easy deposition, low surface roughness, ease of fabrication, besides being more economically viable. DLC has been extensively investigated as a potential material to be applied in optical, biological, mechanical, and electrical fields, to fabricate photonic crystals [3], optical windows [4], protective coatings [5–8], microcircuits [9,10], and biomedical coatings [11–15].

In certain applications, functional properties of DLC films can be achieved by controlling its micro and nanostructure through topography manipulation of the film, often requiring complex patterning methods such as lithographic techniques [16–18]. In this direction, laser surface micromachining is a powerful tool to create precise micro- and nanostructures in several solid materials, including metals [19–21], polymers [22–25], biomaterials [26–29], and semiconductors [30,31]. The fabricated patterns have shown potential functionality in a wide range of applications by manipulating electrical and mechanical properties [32–37], controlling surface wettability [38–40], and optical response [41–45]. It is worth mentioning femtosecond lasers as an attractive tool providing efficiency, precision, and high processing speed, with reduced thermal effects and damages, features that result from the nonlinear light-matter interaction. More specifically, microfabrication carried out with femtosecond laser pulses offers advantages in terms of size features and capability of generating distinct geometries without photomasks, in addition to the facility of processing in different atmospheres [46,47]. In this paper, we investigate the fs-laser microstructuring of DLC, at 800 nm, with the attention focused on the dependence of the threshold

* Corresponding author.
E-mail address: crmendon@ifsc.usp.br (C.R. Mendonça).

https://doi.org/10.1016/j.optmat.2022.112203
Received 27 January 2022; Received in revised form 27 February 2022; Accepted 5 March 2022
Available online 10 March 2022

fluence with the number of pulses, known as the incubation process. The threshold fluence varies from about 0.1 J/cm^2, for a large number of pulses, to 1.0 J/cm^2 for a single pulse, with an evolution that presents a low incubation parameter, i.e, a large number of pulses is needed to induce damage in the material. Considering multiphoton and avalanche ionization as the main mechanisms behind fs-laser processing, we modeled the single-pulse damage threshold fluence and determined the two-photon absorption cross-section of DLC. Lastly, Raman spectroscopy indicates a decrease of the sp^3 fraction and a more ordered phase in the fs-laser processed samples.

2. Experimental

The hydrogenated DLC samples were produced via Chemical Vapor Deposition (CVD), deposited onto glass coverslip substrates (with damage threshold energy much higher than DLC), purchased from CVD VALE®. The deposition approach resulted in DLC films of approximately 500 nm of thickness, estimated by Atomic Force Microscopy (AFM).

Two different laser sources were used at distinct repetition rates to perform the fs-laser micromachining experiments on the DLC samples. The first one was an extended cavity Ti:Sapphire laser oscillator (Femtosource 100XL – Femtolaser®), centered at 800 nm, producing 50-fs laser pulses of maximum energy of 100 nJ at a repetition rate of 5 MHz. The second source was an amplified Ti:Sapphire laser system (Clark – MXR®) emitting 150-fs laser pulses with energy up to 0.5 mJ at a repetition rate of 1 kHz, centered at 775 nm. The combination of these two lasers, of low and high repetition rate, allowed covering a wide range of experimental conditions regarding the pulse superposition. The ablation threshold fluence was measured as a function of the number of incident pulses (N) on the material per surface area.

The laser micromachining was carried out by focusing the laser light into the DLC surface, while the DLC sample was translated. Using a 0.65 NA microscope objective, the laser beam is focused on the surface of the DLC sample, which is positioned on a three-dimensional translation stage controlled via a computer software in LabView®, allowing to move the sample at a constant scan speed, ranging from 1 to 450 μm/s, and accuracy of 50 nm, enabling control of the microstructure size and shape. To vary the pulse energy, a half-wave plate, and a polarizer were used. The entire microfabrication process was monitored in real-time using a CCD camera and backlight illumination.

To study the micromachining incubation process of DLC, two distinct fluence-threshold evaluation methods were employed depending on the laser being used, once the discrepancy on pulse energy between the two laser sources is three orders of magnitude. For the lower repetition rate and higher pulse energy amplified laser system, experiments were carried out using the D-scan method proposed by Samad et al. [48] On the other hand, for the higher repetition rate and lower pulse energy laser oscillator, the zero damage method by Liu [49] was used.

The optical properties of DLC films were analyzed using a UV–vis spectrophotometer (Shimadzu, model UV-1800). To evaluate DLC properties, as well as morphological and structural changes induced by the femtosecond laser micromachining, optical microscopy (Zeiss LSM 700), and Raman spectroscopy (Alpha 300 s A/R – Witec Focus Innovations®) were carried out.

3. Results and discussion

For the higher repetition rate and lower laser pulse energy, the zero damage method (ZDM) was used. In such regime, which corresponds to a large number of pulses per spot, complete removal of material is achieved and optical microscopy was used to measure the width of micromachined lines. The ZDM relies on the damage produced on the sample surface by a laser beam with a Gaussian-intensity profile. In the ZDM, a series of straight grooves are produced with increased pulse energy, and the material ablation threshold fluence (F_{th}) can be obtained by measuring the half-width of the microfabricated lines and fitting such data using [49].

$$r^2 = \frac{w_0^2}{2}\ln\left(\frac{F}{F_{th}}\right) \tag{1}$$

The high repetition rate femtosecond extended-cavity laser (Femtosource 100XL – Femtolaser®: 50-fs, 5 MHz) was used for the micromachining with higher pulse overlap. A set of experiments was performed using a 0.65 NA microscope objective for beam focusing, from 10 μm/s up to 300 μm/s of scanning speed, different pulse energies, and a different number of pulses. Groups of lines of 500 μm separated by ~17 μm were fabricated to evaluate the influence of pulse energy on the width of the lines. Fig. 1a presents an optical microscopy image of typical lines produced with $N = 11300$ with different pulse energies, from 6 up to 16 nJ, using 300 μm/s of scanning speed. From optical microscopy images, for each group of lines produced, it was possible to measure the widths of the fabricated lines, which increase with increasing the pulse energy.

The number of pulses per area can be altered in this method by changing the translation speed (v) of the sample concerning the laser beam and/or the laser repetition rate. Since the laser operates at a high repetition rate (f), the number of pulses superposing (N) at the sample can be calculated by

$$N \cong 1.25\frac{fw_0}{v} \tag{2}$$

in which w_0 is the beam waist. Fig. 1b presents the squared half-width of the produced lines (r) as a function of peak fluence (F) for N = 35000 and 87000 pulses per area. As it can be seen, the half-width of micromachined lines on DLC increases with the peak fluence, varying from approximately 0.6 to 1.3 μm when the peak fluence increases from 0.13 to 0.35 J/cm^2 for 87000 pulses per area (black circles) and from 0.4 to 1.1 μm when the peak fluence increases from 0.2 to 0.5 J/cm^2 for 35000 pulses per area (gray circles).

By fitting the results presented in Fig. 1b with Eq. (1), we have determined the threshold fluence to study the micromachining incubation process of DLC. Such a study was performed using different N, and its results will be shown later in this paper. At this point, it is worth mentioning that for N > 400 the F_{th} ~0.15 J/cm^2.

The D-scan method performed with the low repetition rate femtosecond amplifier (Clark – MRX®: 150-fs, 1 kHz) was used for the micromachining with lower pulse overlap, covering N from approximately 20 to 400 pulses per area. For this regime, there can be ablation or structural only modification of the material. Therefore, we used scanning electron microscopy to evaluate the changes induced on the sample, by inspecting the D-scan profile. Peak fluence varied from 43 up to 90 J/cm^2 and scan speed from 0.05 up to 1 mm/s to control the number of pulses per spot. The characteristic D-scan profile was obtained, from which the maximum half-width (ρ_{max}) of the side lobes were measured and the F_{th} calculated. Typical D-scan profiles are shown in Fig. 2.

The D-scan method is based on a diagonal translation of the sample with respect to the laser beam focus, exposing it to a variety of laser fluencies at different regions, forming a two-lobe type pattern onto the sample. Ablation threshold fluence (F_{th}) is determined by measuring the pulse energy (E_0) and the maximum half-width (ρ_{max}) of the side lobes and inputting in the expression [50].

$$F_{th} \cong 0.117\frac{E_0}{e\pi\rho_{max}^2} \tag{3}$$

In this method, the number of pulse superposition (N) is controlled by the speed (v) with which the sample is translated perpendicularly to the beam propagation and the laser repetition rate (f), and can be calculated by [50].

$$N = \vartheta_3\left(0, e^{-(v/f\rho_{max})^2}\right) \tag{4}$$

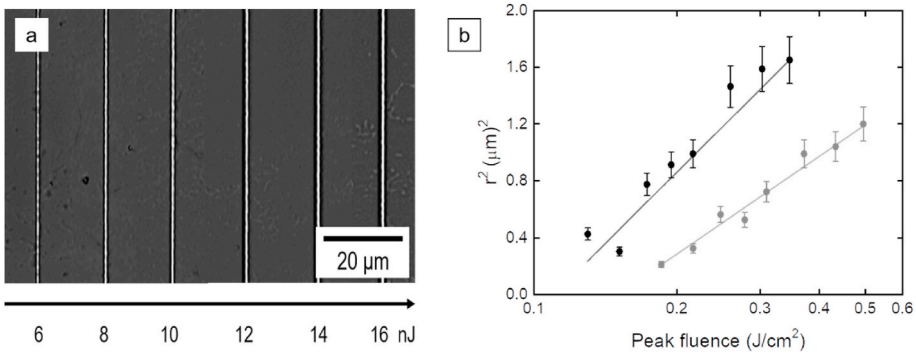

Fig. 1. a) Optical images of lines produced with 11300 pulses in different energies, from 6 to 16 nJ, using 300 μm/s of scanning speed. b) Squared half-width of micromachined lines as a function of the pulse peak fluence, fitting curves for N = 35000 (gray circles) and N = 87000 (black circles) obtained from femtosecond micromachining experiments.

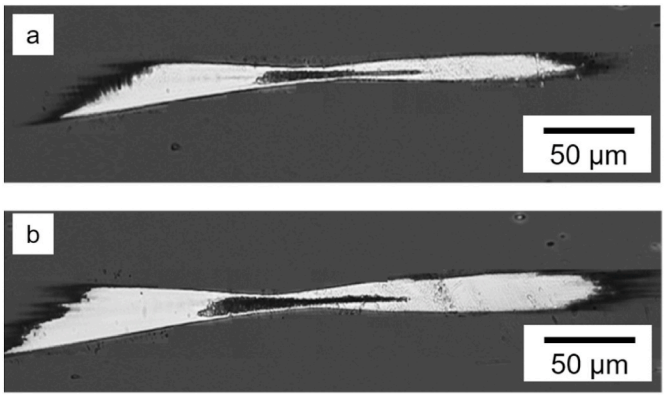

Fig. 2. D-scan profile micromachined with (a) 43 J/cm^2 and 0.1 mm/s, and (b) 90 J/cm^2 and 0.5 mm/s.

Because the D-scan method requires a fluence high enough to ablate the material even when it is not at the laser beam focal plane, this experiment was carried out using the higher energy pulses from the amplified laser system. The F_{th} results obtained through the D-scan for different N values, together with the ones found by the ZDM method, will be shown later when the incubation effect is discussed. It is interesting to note, however, that through the D-scan that F_{th} varies from ~0.5 J/cm^2 to 1 J/cm^2 for N in the range 20–400.

Having measured the damage threshold fluence for a wide range of pulse overlap, we were able to generate the incubation curve (Fig. 3). To validate the use of D-scan and ZDM, the threshold fluence for 400 pulses was measured using both methods. The obtained threshold fluences were very similar, confirming that the two methods give equivalent results, within the experimental error. In Fig. 3, for N = 400, the red circle corresponds to the data measured by ZDM. The incubation phenomenon can be observed in many different materials and it's modeled by empirical expressions assuming the accumulation of defects is exponential or probabilistic. The former model is mostly applied to dielectrics, while the latter fits better incubation curves for metals. Since DLC is a dielectric, we chose the exponential model to fit our incubation data, which follows the expression

$$F_{th,N} = \left(F_{th,1} - F_{th,\infty}\right)e^{-k(N-1)} + F_{th,\infty} \tag{5}$$

where $F_{th,1}$ and $F_{th,\infty}$ are the single and infinite pulse ablation threshold fluence, N is the number of pulses per spot and k is the incubation parameter. Incubation effect in DLC from femtosecond laser micromachining is displayed in Fig. 3, along with its model, from which k was determined to be (0.004 ± 0.001), $F_{th,1}$ and $F_{th,\infty}$ as (1.0 ± 0.1) and (0.13 ± 0.04) J/cm^2 , respectively. Single-pulse threshold fluence found

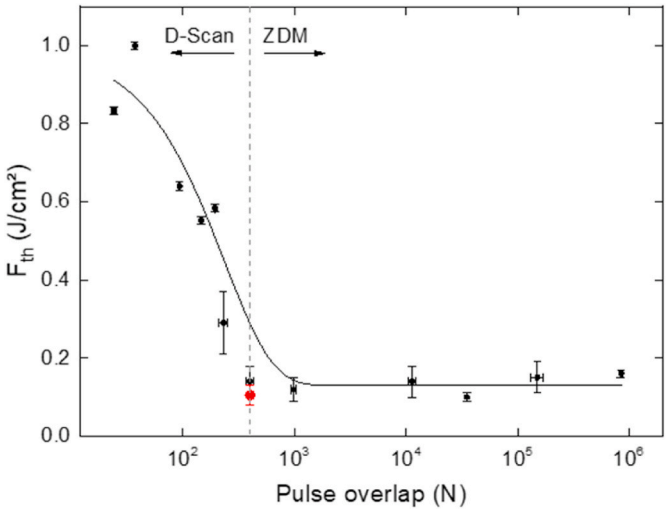

Fig. 3. Incubation effect of DLC thin film. Damage threshold fluence as a function of the number of pulses per spot and exponential model-fitting curve. The red circle corresponds to the data measured by ZDM, to validate the used of both methods. The dashed lines and arrows indicate the regions measured with each of the methods.

here is in the same order as a previous study reported in the literature [51]. Minor differences may be due to DLC film composition and sample surface quality. The incubation parameter refers to the dynamics of the incubation process and such a low value for k indicates that incubation in DLC evolves slowly, requiring a large number of overlapping pulses to damage the material. It is interesting to observe that the incubation parameter k for DLC is one order of magnitude smaller than the ones observed for other dielectric transparent materials [50,52]. The greater resistance to optical damage of DLC is probably related to its distinguished thermal and mechanical properties.

Further investigation of the fs-micromachining process of DLC was performed by a theoretical model which describes the electron density (n), produced by a fs-laser pulse through multiphoton and avalanche ionization alone [53], given by

$$n = \sigma_m \left(\frac{\lambda}{hc}\right)^m \frac{N_s I_0^m \tau}{2} \left(\frac{\pi}{mln2}\right)^{1/2} \exp\left[\frac{\alpha I_0 \tau}{4}\left(\frac{\pi}{ln2}\right)^{1/2}\right] \tag{6}$$

where m is the number of photons related to the multiphoton ionization, σ_m is the m-photon cross-section, N_s is the solid atom density, λ is the laser wavelength, h is Planck's constant, c is the speed of light, I_0 is the laser peak intensity, τ is the laser pulse duration and finally $2/\alpha$ is a scale fluence which dictates the relevance of the avalanche ionization. Hence,

one can determine the single-pulse damage threshold fluence through

$$F_{th,1} = (I_0\tau / 2)(\pi/ln2)^{1/2} \quad (7)$$

in which the value of I_0 is taken when the electron density reaches its critical point (n_{cr}) for which damage starts to occur.

The number of photons (m) required by the multiphoton ionization process can be determined through the material's energy gap, found by the Tauc/Davis-Mott model [54–56]. According to the model, $(\alpha h\nu)^{1/b} = A(h\nu - E_g)$, where α is the absorption coefficient, E_g is the energy gap, A is a constant and b indicates whether the electronic transition is allowed or forbidden or if it is direct or indirect. As such, when $(\alpha h\nu)^{1/b}$ is plotted as a function of $h\nu$, as seen in Fig. 4, one can extrapolate E_g from the linear portion of the graph. However, since the Tauc/Davis-Mott plot of DLC presents two linear regions, the energy gap can be estimated through the intersection of the two fitted linear lines [57], which yields a value of 2 eV. Thus, since the fs-laser pulse wavelength is 800 nm ($\sim$ 1.55 eV), it would require a value of $m = 2$ photons for an electron to be excited to the conduction band through multiphoton ionization.

Since Eq. (6) only considers multiphoton and avalanche ionization as the electron density generation process, the Keldysh parameter was determined [58]. It ascertains if either tunneling or multiphoton ionization is predominant, since they are considered to be the same effect, only being distinguished by a low and high-frequency regime, respectively. Thus, the Keldysh parameter (γ_K) given by

$$\gamma_K = \frac{\omega}{e}\sqrt{\frac{m_e\varepsilon_0 c n_0 E_g}{I_0}} \quad (8)$$

where ω is the angular optical frequency, m_e and e are the electron's mass and charge, n_0 is the material's refractive index, and ε_0 is the vacuum permittivity, yielded a value of $\gamma_K = (2.3 \pm 0.1)$, which corresponds to the multiphoton regime, since $\gamma_K > 1.5$ [59], thus validating the usage of the model.

Finally, by using $n_{cr} = 2 \times 10^{27}$ electrons/m^3 [60] and the two-photon cross-section of diamond of $\sigma_2 = (7 \pm 3) \times 10^{-60}$ m^{4}s^{1}photon^{-1} [61] due to the lack of data on DLC's two-photon absorption coefficient in the literature, we determined $F_{th,1} = (0.5 \pm 0.2)$ J/cm^2, which is in good agreement with the experimental value of (1.0 $\pm$ 0.1) J/cm^2. In order to reproduce an even better single pulse-damage threshold fluence, we determined a laser peak intensity of $I_0 = (6.3 \pm 0.6) \times 10^{16}$ W/m^2 from Eq. (6) through the $F_{th,1}$ experimental value, and estimated σ_2 of $(1.5 \pm 0.5) \times 10^{-60}$ m^{4}s^{1}photon^{-1} from Eq. (6), that is consistent with the one found for diamond. Although such results have been obtained for thin films, given the high absorption of DLC at the laser wavelength used, micromachining would be confined to a thin layer of a DLC bulk sample; thus the results described here could be extrapolated to the bulk.

Carbon-based materials, such as diamond, carbon nanotubes, graphite, and DLC films have been thoroughly studied via Raman scattering so that their vibrational modes are well characterized [62–65]. Raman spectra of hydrogenated DLC samples are first treated with linear background removal and then deconvoluted in two Gaussians. Fig. 5 presents the Raman spectrum of DLC thin films under 514 nm excitation, along with the deconvoluted peaks. The G peak centered at 1548 cm^{-1} is assigned to zone center phonons of E_{2g} symmetry [66,67], while the D peak at 1349 cm^{-1} is a breathing mode A_{1g} symmetry involving phonons near the K-point zone [54].

In order to investigate structural modifications produced by ultrashort pulse micromachining on the irradiated DLC film, Raman spectroscopy was performed on the line center, as well as on the edges of the line fabricated using fluence of 0.14 J/cm^2 and about 11000 pulses/spot. For comparison, Raman spectroscopy was performed using the same parameters on the non-irradiated DLC film. On the center of the line, the Raman signal is extremely weak in the region between 1400 and 2000 cm-1, showing the most prominent Raman bands of the glass coverslip substrates, which was expected because DLC was ablated. The Raman spectrum of irradiated DLC film on the line edges, that presets a depressed region surrounded by resolidified material, displayed in Fig. 6, is also featured by G and D peaks, centered at 1559 cm-1 and 1388 cm-1, respectively. It is worth noting that in comparison to non-irradiated regions, the Raman spectra of remaining areas of the microstructures does not show any differences.

Disordered carbons have sp^3 and sp^2 sites, and their Raman spectrum depends on clustering of the sp^2 phase, bond disorder, the presence of sp^2 rings or chains, and the sp^2/sp^3 ratio, which can be evaluated by the ratio between D and G bands (I_D/I_G), since there is a dependency on the ordering of sp^2 sites and the fraction of sp^3 sites.) [63]. The I_D/I_G the hydrogenated DLC sample studied here is 0.42 (Fig. 5). After the fs-laser interaction, we obtained $I_D/I_G = 0.81$ (Fig. 6), higher than the one for the non-irradiated DLC film, which is in accordance with a decrease in the amorphization, and a change in the G peak position, indicating a more ordered phase. Such a process is in agreement with others studies

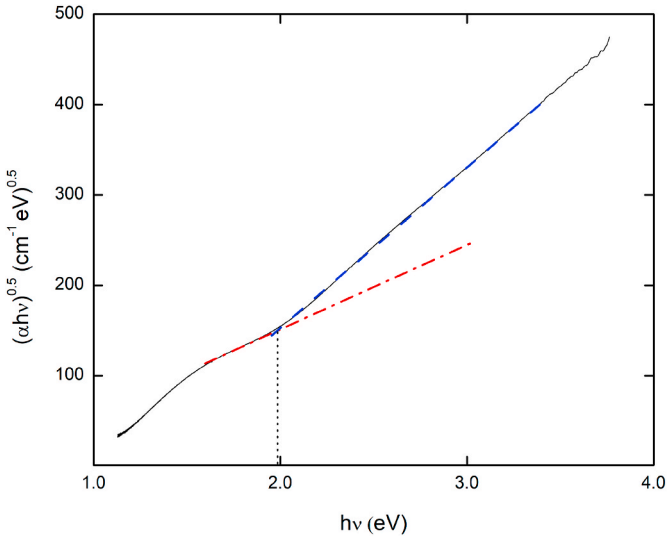

Fig. 4. Tauc/Davis-Mott plot of DLC. The intersection of the two linear portions (blue dashed line and red dashed line) determines the energy gap of 2 eV.

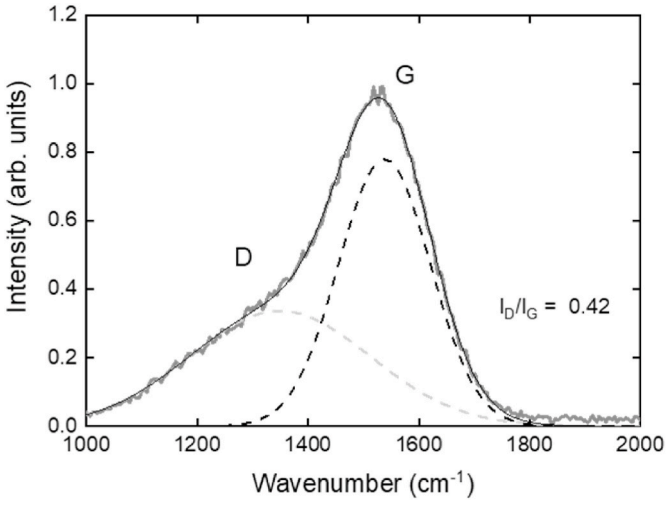

Fig. 5. Raman spectrum of DLC thin films under 514 nm excitation (gray line). Dashed lines (– – –) and (——) correspond to Gaussian deconvoluted peaks centered at 1349 cm^{-1} and 1548 cm^{-1}, while the black line corresponds to their sum.

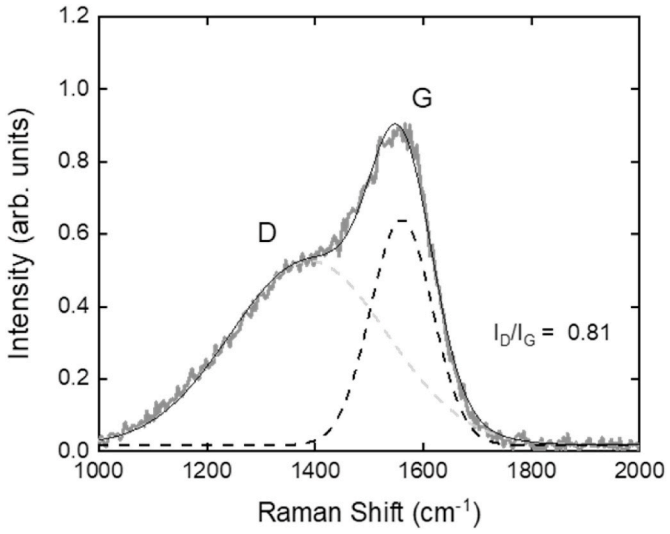

Fig. 6. Raman spectrum under 514 nm excitation (gray line) of fs-laser irradiated DLC thin film with fluence close to its damage threshold. Lines (– – –) and (——) correspond to Gaussian deconvoluted bands centered at 1416 cm^{-1} and 1560 cm^{-1}, while the black line corresponds to their sum.

involving laser microfabrication on DLC films [68,69].

4. Conclusion

We studied the incubation process in DLC films upon fs-laser microstructuring at 800 nm. We have determined the material threshold fluence as (1.0 ± 0.1) J/cm^2 for a single pulse, and (0.13 ± 0.04) J/cm^2 when a large number of pulses is incident on the sample. Our results showed a small incubation factor, which indicates that the decrease in threshold fluence occurs slowly with the number of pulses, i.e., a large number of pulses is required to observe a significant decrease in threshold fluence, which reveal that the laser induced defects generation in DLC evolves slowly with the number of pulses. Using a model that considers multiphoton (two-photons) and avalanche ionization as the main process behind DLC fs-laser processing, we estimated its two-photon absorption cross-section as $\sigma_2 = (1.5 \pm 0.5) \times 10^{-60}$ $m^4s^1photon^{-1}$, a value which is close to the one exhibited by a diamond. Finally, Raman spectroscopy indicates a decrease of the sp^3 fraction and a more ordered phase in the irradiated regions of the DLC sample.

CRediT authorship contribution statement

Lucas K. Nolasco: Conceptualization, Methodology, Investigation, Writing – original draft. **Flávio P. Almeida:** Conceptualization, Methodology, Investigation, Writing – original draft. **Gustavo F.B. Almeida:** Conceptualization, Investigation, Writing – original draft. **Juliana M.P. Almeida:** Conceptualization, Investigation, Writing – original draft. **Valmor R. Mastelaro:** Resources, Investigation, Writing – original draft. **Kelly T. Paula:** Investigation, Writing – original draft, Writing – review & editing. **Cleber R. Mendonça:** Conceptualization, Methodology, Investigation, Supervision, Project administration, Funding acquisition, Writing – original draft, Writing – review & editing.

Declaration of competing interest

The authors declare the following financial interests/personal relationships which may be considered as potential competing interests: Cleber R. Mendonca reports financial support was provided by State of Sao Paulo Research Foundation. Cleber R. Mendonca reports financial support was provided by National Council for Scientific and Technological Development. Cleber R. Mendonca reports was provided by Coordination of Higher Education Personnel Improvement.

Acknowledgments

We acknowledge FAPESP (2018/11283-7), CNPq, and CAPES for financial support.

References

[1] J. Robertson, Diamond-like carbon, Pure Appl. Chem. 66 (1994) 1789–1796.
[2] J. Robertson, Review Properties of diamond-like carbon, Surf. Coating. Technol. 50 (1992) 185–203.
[3] J.G. Yun, D.H. Jung, H.J. Kim, W.S. Choi, B.Y. Hong, S. Noda, B.S. Song, Microelectronic Engineering Fabrication of diamond-like carbon-based two-dimensional photonic crystals, Microelectron. Eng. 126 (2014) 99–102, https://doi.org/10.1016/j.mee.2014.06.030.
[4] J.G. Yun, D.H. Jung, H.J. Kim, W.S. Choi, B.Y. Hong, S. Noda, B.S. Song, Microelectronic Engineering Fabrication of diamond-like carbon-based two-dimensional photonic crystals, Microelectron. Eng. 126 (2014) 99–102, https://doi.org/10.1016/j.mee.2014.06.030.
[5] F.M. Kimock, B.J. Knapp, Commercial applications of ion beam deposited diamond-like carbon (DLC) coatings, Surf. Coating. Technol. 56 (1993) 273–279.
[6] A.A. Voevodin, M.S. Donley, J.S. Zabinski, Pulsed laser deposition of diamond-like carbon wear protective coatings : a review, 1, Surf. Coating. Technol. 92 (1997) 42–49.
[7] N. Dwivedi, S. Kumar, S. Singh, H.K. Malik, Oxygen modified diamond-like carbon as window layer for amorphous silicon solar cells, Sol. Energy 86 (2012) 220–230, https://doi.org/10.1016/j.solener.2011.09.025.
[8] F. Piazza, D. Grambole, D. Schneider, C. Casiraghi, A.C. Ferrari, J. Robertson, Protective diamond-like carbon coatings for future optical storage disks, 14, 2005, pp. 994–999, https://doi.org/10.1016/j.diamond.2004.12.028.
[9] E. Liu, H.W. Kwek, Electrochemical performance of diamond-like carbon thin films, 516, 2008, pp. 5201–5205, https://doi.org/10.1016/j.tsf.2007.07.089.
[10] J.K. Luo, Y.Q. Fu, H.R. Le, J.A. Williams, S.M. Spearing, Diamond and Diamond-like Carbon MEMS, 2007, p. 147, https://doi.org/10.1088/0960-1317/17/7/S12.
[11] G. Dearnaley, J.H. Arps, Biomedical applications of diamond-like carbon (DLC) coatings: a review, Surf. Coating. Technol. 200 (2005) 2518–2524, https://doi.org/10.1016/j.surfcoat.2005.07.077.
[12] L. Anne Thomson, F.C. Law, N. Rushton, J. Franks, Biocompatibility of diamond-like carbon coating, Biomaterials 12 (1991) 37–40, https://doi.org/10.1016/0142-9612(91)90129-X.
[13] A. Grill, Diamond-like carbon coatings as biocompatible materials - an overview, Diam. Relat. Mater. 12 (2003) 166–170, https://doi.org/10.1016/S0925-9635(03)00018-9.
[14] C.C. Wachesk, S.H. Seabra, T.A.T. Dos Santos, V.J. Trava-Airoldi, A.O. Lobo, F. R. Marciano, In vivo biocompatibility of diamond-like carbon films containing TiO2 nanoparticles for biomedical applications, J. Mater. Sci. Mater. Med. 32 (2021), https://doi.org/10.1007/s10856-021-06596-6.
[15] Y. Manome, T. Tachibana, M. Hiratsuka, K. Sato, Y. Ohgoe, K. Hirakuri, Osteoblastic MC3T3-E1 cells on diamond-like carbon-coated silicon plates: field emission scanning electron microscopy data, Data Brief 38 (2021), 107385, https://doi.org/10.1016/j.dib.2021.107385.
[16] S.M. Yang, S.G. Jang, D.G. Choi, S. Kim, H.K. Yu, Nanomachining by colloidal lithography, Small 2 (2006) 458–475, https://doi.org/10.1002/smll.200500390.
[17] A. Kosiorek, W. Kandulski, P. Chudzinski, K. Kempa, M. Giersig, Shadow nanosphere lithography: simulation and experiment, Nano Lett. 4 (2004) 1359–1363, https://doi.org/10.1021/nl049361t.
[18] H.W. Deckman, J.H. Dunsmuir, Natural lithography, Appl. Phys. Lett. 41 (1982) 377–379, https://doi.org/10.1063/1.93501.
[19] H. Qi, H. Lai, Micromachining of metals and thermal barrier coatings using a 532 nm nanosecond fiber laser, Phys. Procedia 39 (2012) 603–612, https://doi.org/10.1016/j.phpro.2012.10.079.
[20] J. Heo, H. Min, M. Lee, Laser micromachining of permalloy for fine metal mask, Int. J. Precis. Eng. Manuf. - Green Technol. 2 (2015) 225–230, https://doi.org/10.1007/s40684-015-0026-7.
[21] K.M. Tanvir Ahmmed, C. Grambow, A.M. Kietzig, Fabrication of micro/nano structures on metals by femtosecond laser micromachining, Micromachines 5 (2014) 1219–1253, https://doi.org/10.3390/mi5041219.
[22] L. Ding, D. Jani, J. Linhardt, J.F. Künzler, S. Pawar, G. Labenski, T. Smith, W. H. Knox, Large enhancement of femtosecond laser micromachining speed in dye-doped hydrogel polymers, Opt Express 16 (2008), 21914, https://doi.org/10.1364/oe.16.021914.
[23] N.C. Nayak, Y.C. Lam, C.Y. Yue, A.T. Sinha, CO2-laser micromachining of PMMA: the effect of polymer molecular weight, J. Micromech. Microeng. 18 (2008), https://doi.org/10.1088/0960-1317/18/9/095020.
[24] V.V. Kancharla, S. Chen, Fabrication of biodegradable polymeric micro-devices using laser micromachining, Biomed. Microdevices 4 (2002) 105–109, https://doi.org/10.1023/A:1014679013888.
[25] C.R. Mendonca, D.S. Correa, F. Marlow, T. Voss, P. Tayalia, E. Mazur, Three-dimensional fabrication of optically active microstructures containing an electroluminescent polymer three-dimensional fabrication of optically active microstructures containing an electroluminescent polymer. https://doi.org/10.1063/1.3232207, 2009.

[26] C. Hallgren, H. Reimers, D. Chakarov, J. Gold, A. Wennerberg, An in vivo study of bone response to implants topographically modified by laser micromachining, Biomaterials 24 (2003) 701–710, https://doi.org/10.1016/S0142-9612(02)00266-1.
[27] A. Kurella, N.B. Dahotre, Review paper: surface modification for bioimplants: the role of laser surface engineering. https://doi.org/10.1177/0885328205052974, 2005.
[28] S. Nizamoglu, M.C. Gather, S.H. Yun, All-biomaterial laser using vitamin and biopolymers, Adv. Mater. 25 (2013) 5943–5947, https://doi.org/10.1002/adma201300818.
[29] C.A. Aguilar, Y. Lu, S. Mao, S. Chen, Direct micro-patterning of biodegradable polymers using ultraviolet and femtosecond lasers, Biomaterials 26 (2005) 7642–7649, https://doi.org/10.1016/j.biomaterials.2005.04.053.
[30] Q. Zhao, M. Lukitsch, J. Xu, G. Auner, Development of wide bandgap semiconductor photonic device structures by excimer laser micromachining, Mater. Res. Soc. Symp. Proc. 595 (2000) 1–6, https://doi.org/10.1557/s1092578300005172.
[31] D. Zhang, B. Gökce, S. Sommer, R. Streubel, S. Barcikowski, Debris-free rear-side picosecond laser ablation of thin germanium wafers in water with ethanol, Appl. Surf. Sci. 367 (2016) 222–230, https://doi.org/10.1016/j.apsusc.2016.01.071.
[32] S. Chae, A. Yi, C. Park, W.S. Chang, H.H. Lee, J. Choi, H.J. Kim, Using femtosecond laser irradiation to enhance the vertical electrical properties and tailor the morphology of a conducting polymer blend film, ACS Appl. Mater. Interfaces 9 (2017) 24422–24427, https://doi.org/10.1021/acsami.7b05937.
[33] X.Y. Yu, Z.H. Lv, C.H. Li, X. Han, J.H. Zhao, The optical and electrical properties of Co-doped black silicon textured by a femtosecond laser and its application to infrared light sensing, IEEE Sensor. J. 16 (2016) 5227–5231, https://doi.org/10.1109/JSEN.2016.2564500.
[34] J. Cui, Y. Cheng, J. Zhang, H. Mei, X. Wang, Femtosecond laser irradiation of carbon nanotubes to metal electrodes, Appl. Sci. 9 (2019), https://doi.org/10.3390/app9030476.
[35] K.T. Paula, M.V. Santos, M.H.M. Facure, M.B. Andrade, F.L. Araújo, D.S. Correa, S. J.L. Ribeiro, C.R. Mendonça, Laser patterning and induced reduction of graphene oxide functionalized silk fibroin, Opt. Mater. (Amst). 99 (2020), 109540, https://doi.org/10.1016/j.optmat.2019.109540.
[36] S. Jakob, M.J. Pfeifenberger, A. Hohenwarter, R. Pippan, Femtosecond laser machining for characterization of local mechanical properties of biomaterials: a case study on wood, Sci. Technol. Adv. Mater. 18 (2017) 574–583, https://doi.org/10.1080/14686996.2017.1360751.
[37] P. Kongsuwan, H. Wang, S. Vukelic, Y.L. Yao, Characterization of morphology and mechanical properties of glass interior irradiated by femtosecond laser, J. Manuf. Sci. Eng. Trans. ASME. 132 (2010), https://doi.org/10.1115/1.4002062, 410091–4100910.
[38] C. Lanara, A. Mimidis, E. Stratakis, Femtosecond laser fabrication of stable hydrophilic and anti-corrosive steel surfaces, Materials (Basel) 12 (2019) 1–9, https://doi.org/10.3390/ma12203428.
[39] Z.K. Wang, H.Y. Zheng, Y.C. Lam, Investigation on femtosecond laser irradiation energy in inducing hydrophobic polymer surfaces, Appl. Surf. Sci. 257 (2011) 10427–10433, https://doi.org/10.1016/j.apsusc.2011.06.123.
[40] K.T. Paula, K.L.C. Silva, A.V.A. Mattos, M.B. de Andrade, R.C. Sanfelice, D. T. Balogh, C.R. Mendonça, Controlling surface wettability in methacrylic copolymer containing azobenzene by fs-laser microstructuring, Opt. Mater. (Amst). 116 (2021), 111083, https://doi.org/10.1016/j.optmat.2021.111083.
[41] M.V. Santos, S.N.C. Santos, R.J. Martins, J.M.P. Almeida, K.T. Paula, G.F. B. Almeida, S.J.L. Ribeiro, C.R. Mendonça, Femtosecond direct laser writing of silk fibroin optical waveguides, J. Mater. Sci. Mater. Electron. (2019), https://doi.org/10.1007/s10854-019-01406-w.
[42] Y. Wang, D.N. Wang, M. Yang, W. Hong, P. Lu, Refractive index sensor based on a microhole in single-mode fiber created by the use of femtosecond laser micromachining, Opt. Lett. 34 (2009) 3328, https://doi.org/10.1364/ol.34.003328.
[43] M. Kamata, M. Obara, R.R. Gattass, L.R. Cerami, E. Mazur, Optical vibration sensor fabricated by femtosecond laser micromachining, Appl. Phys. Lett. 87 (2005) 1–4, https://doi.org/10.1063/1.2008362.
[44] A.G. Ciriolo, R.M. Vázquez, A. Roversi, A. Frezzotti, C. Vozzi, R. Osellame, S. Stagira, Femtosecond laser-micromachining of glass micro-chip for high order harmonic generation in gases, Micromachines 11 (2020) 1–9, https://doi.org/10.3390/mi11020165.
[45] S.N.C. Santos, G.F.B. Almeida, J.M.P. Almeida, A.C. Hernandes, C.R. Mendonça, Waveguides fabrication by femtosecond laser in Tb3+/Yb3+ doped CaLiBO glasses, Opt Laser. Technol. 140 (2021), 107030, https://doi.org/10.1016/j.optlastec.2021.107030.
[46] M.V. Santos, K.T. Paula, M.B. De Andrade, E.M. Gomes, L.F. Marques, S.J. L. Ribeiro, C.R. Mendonça, Direct femtosecond laser printing of silk fibroin microstructures, ACS Appl. Mater. Interfaces 12 (2020) 50033–50038, https://doi.org/10.1021/acsami.0c13482.
[47] J.M.P. Almeida, K.T. Paula, C.B. Arnold, C.R. Mendonça, Sub-wavelength self-organization of chalcogenide glass by direct laser writing, Opt. Mater. (Amst). 84 (2018) 259–262, https://doi.org/10.1016/j.optmat.2018.06.068.
[48] R.E. Samad, N.D. Vieira, Geometrical method for determining the surface damage threshold for femtosecond laser pulses, Laser Phys. 16 (2006) 336–339, https://doi.org/10.1134/s1054660x06020228.
[49] J.M. Liu, Simple technique for measurements of pulsed Gaussian-beam spot sizes, Opt. Lett. 7 (1982) 196–198, https://doi.org/10.1364/OL.7.000196.
[50] L.M. Machado, R.E. Samad, W. de Rossi, N.D.V. Junior, D-Scan measurement of ablation threshold incubation effects for ultrashort laser pulses, Opt Express 20 (2012) 4114, https://doi.org/10.1364/oe.20.004114.
[51] Y. Dong, H. Sakata, P. Molian, Femtosecond pulsed laser ablation of diamond-like carbon films on silicon, Appl. Surf. Sci. 252 (2005) 352–357, https://doi.org/10.1016/j.apsusc.2005.01.008.
[52] L. Qi, K. Nishii, M. Yasui, H. Aoki, Y. Namba, Femtosecond laser ablation of sapphire on different crystallographic facet planes by single and multiple laser pulses irradiation, Opt Laser. Eng. 48 (2010) 1000–1007, https://doi.org/10.1016/j.optlaseng.2010.05.006.
[53] B. Stuart, M. Feit, S. Herman, A. Rubenchik, B. Shore, M. Perry, Nanosecond-to-femtosecond laser-induced breakdown in dielectrics, Phys. Rev. B - Condens. Matter Mater. Phys. 53 (1996) 1749–1761, https://doi.org/10.1103/PhysRevB.53.1749.
[54] E.A. Davis, N.F. Mott, Conduction in non-crystalline systems V. Conductivity, optical absorption and photoconductivity in amorphous semiconductors, Philos. Mag. 22 (1970) 903–922, https://doi.org/10.1080/14786437008221061.
[55] J. Tauc, R. Grigorovici, A. Vancu, Optical properties and electronic structure of amorphous germanium, Phys. Status Solidi 15 (1966) 627–637, https://doi.org/10.1002/pssb.19660150224.
[56] J. Tauc, Optical properties and electronic structure of amorphous Ge and Si, Mater. Res. Bull. 3 (1968) 37–46, https://doi.org/10.1016/0025-5408(68)90023-8.
[57] P. Makuła, M. Pacia, W. Macyk, How to correctly determine the band gap energy of modified semiconductor photocatalysts based on UV-vis spectra, J. Phys. Chem. Lett. 9 (2018) 6814–6817, https://doi.org/10.1021/acs.jpclett.8b02892.
[58] L.V. Keldysh, Ionization in the field of a strong electromagnetic wave, Sov. Phys. JETP 20 (1965) 1945–1957.
[59] C.B. Schaffer, A. Brodeur, E. Mazur, Laser-induced breakdown and damage in bulk transparent materials induced by tightly focused femtosecond laser pulses, Meas. Sci. Technol. 12 (2001) 1784–1794, https://doi.org/10.1088/0957-0233/12/11/305.
[60] L.K. Nolasco, G.F.B. Almeida, T. Voss, C.R. Mendonça, Femtosecond laser micromachining of GaN using different wavelengths from near-infrared to ultraviolet, J. Alloys Compd. 877 (2021), 160259, https://doi.org/10.1016/j.jallcom.2021.160259.
[61] J.M.P. Almeida, C. Oncebay, J.P. Siqueira, S.R. Muniz, L. De Boni, C.R. Mendonça, Nonlinear optical spectrum of diamond at femtosecond regime, Sci. Rep. 7 (2017), https://doi.org/10.1038/s41598-017-14748-4.
[62] D.R. Tallant, J.E. Parmeter, M.P. Siegal, R.L. Simpson, The thermal stability of diamond-like carbon, Diam. Relat. Mater. 4 (1995) 191–199, https://doi.org/10.1016/0925-9635(94)00243-6.
[63] A.C. Ferrari, Determination of bonding in diamond-like carbon by Raman spectroscopy, Diam. Relat. Mater. 11 (2002) 1053–1061, https://doi.org/10.1016/S0925-9635(01)00730-0.
[64] S. Ushiba, S. Shoji, K. Masui, P. Kuray, J. Kono, S. Kawata, 3D microfabrication of single-wall carbon nanotube/polymer composites by two-photon polymerization lithography, Carbon N. Y. 59 (2013) 283–288, https://doi.org/10.1016/j.carbon.2013.03.020.
[65] G. Irmer, A. Dorner-Reisel, Micro-Raman studies on DLC coatings, Adv. Eng. Mater. 7 (2005) 694–705, https://doi.org/10.1002/adem.200500006.
[66] H. Pang, X. Wang, G. Zhang, H. Chen, G. Lv, S. Yang, Characterization of diamond-like carbon films by SEM, XRD and Raman spectroscopy, Appl. Surf. Sci. 256 (2010) 6403–6407, https://doi.org/10.1016/j.apsusc.2010.04.025.
[67] Y. Li, G. Zhang, X. Hou, D. Deng, Synthesis and tribological properties of diamond-like carbon films by electrochemical anode deposition, Appl. Surf. Sci. 258 (2012) 6527–6530, https://doi.org/10.1016/j.apsusc.2012.03.070.
[68] G. Dumitru, V. Romano, H.P. Weber, S. Pimenov, T. Kononenko, M. Sentis, J. örg Hermann, S. Bruneau, Femtosecond laser ablation of diamond-like carbon films, Appl. Surf. Sci. 222 (2004) 226–233, https://doi.org/10.1016/j.apsusc.2003.08.031.
[69] G. Miyaji, K. Miyazaki, Ultrafast dynamics of periodic nanostructure formation on diamondlike carbon films irradiated with femtosecond laser pulses, Appl. Phys. Lett. 89 (2006) 1–4, https://doi.org/10.1063/1.2374858.